JOURNAL OF Materials CHEMISTRY

A new class of three dimensional D–π–A trigonal cryptand derivatives for second-order nonlinear optics†

Pritam Mukhopadhyay,[a] Parimal K. Bharadwaj,*[a] G. Savitha,[a] Anu Krishnan[b] and Puspendu K. Das*[b]

[a]*Department of Chemistry, Indian Institute of Technology, Kanpur 208016, India. E-mail: pkb@iitk.ac.in*
[b]*Department of Inorganic and Physical Chemistry, Indian Institute of Science, Bangalore 560012, India*

Received 19th March 2002, Accepted 9th April 2002
First published as an Advance Article on the web 15th May 2002

Synthesis, crystal structures, linear and nonlinear optical properties of tris D–π–A cryptand derivatives with C_3 symmetry are reported. Three fold symmetry inherent in the cryptand molecules has been utilized for designing these molecules. Molecular nonlinearities have been measured by hyper-Rayleigh scattering (HRS) experiments. Among the compounds studied, $\mathbf{L_1}$ adopts non-centrosymmetric crystal structure. Compounds $\mathbf{L_1}$, $\mathbf{L_2}$, $\mathbf{L_3}$ and $\mathbf{L_4}$ show a measurable SHG powder signal. These molecules are more isotropic and have significantly higher melting points than the classical *p*-nitroaniline based dipolar NLO compounds, making them useful for further device applications. Besides, different acceptor groups can be attached to the cryptand molecules to modulate their NLO properties.

Introduction

The design and synthesis of organic molecules exhibiting second-order nonlinear optical (NLO) properties have been motivated by their tremendous potential for application in telecommunications, optical computing and data storage.[1] Advantages of using organic molecules as NLO materials stem from the fact that they can be designed to optimize the desired NLO property. At the molecular level, compounds likely to exhibit large values of molecular hyperpolarizability, β must have polarizable electrons (*e.g.*, π-electrons) spread over a large distance. It has been shown that extended π systems with terminal donor acceptor substituents exhibit large β values.[2] However, a major problem associated with these traditional dipolar chromophores is the nonlinearity–transparency trade-off, such that the desirable increase in second-order polarizability is accompanied by a bathochromic shift[3] of the electronic transition, leading to undesirable dispersion, fluorescence as well as re-absorption effects. Although β of a molecule is closely related to the bulk second-order nonlinearity, $\chi^{(2)}$ in the solid state, large values of β do not necessarily lead to high $\chi^{(2)}$. The large dipole moment in pNA like dipolar donor acceptor molecules make them pack in an *anti*-parallel fashion leading to centrosymmetry which is detrimental for SHG. Moreover, these 1D molecules, because of their anisotropic structure have small off-diagonal tensor components and produce polarized SH light.

Strategies have been evolved during the past decade to circumvent these drawbacks by extending the charge-transfer dimension from one to two or three.[4] The idea is to arrange more symmetrical molecules in isotropic but non-centrosymmetric arrays to achieve large nonlinearity. Investigations on more isotropic molecules belonging to an octupolar group (a multipolar group, in general) such as the D_{3h} group or the tetrahedral cubic group T_d or to a quadrupolar group such as the orthorhombic 222 group have been made. For example, 2,4,6-triamino-1,3,5-trinitrobenzene (TATB), the trigonal analogue of the dipolar pNA molecule has generated a lot of interest after it was found that TATB shows[5] a powder efficiency of 3 × U in spite of having crystallized in a triclinic $P\bar{1}$ centrosymmetric space group. This apparent contradiction was finally resolved when Martin *et al.*[6a] reported that structural modulation on the *c*-axis of the unit cell gives rise to SHG activity in TATB. The two and three-dimensional (2D and 3D) chromophores with D_3, D_{3h} or T_d symmetry, termed as octupolar molecules,[7] offer several advantages: (i) they can be made more transparent *via* design, (ii) they can exhibit large second order nonlinearity at no cost to transparency, and (iii) they have greater probability of crystallization in a non-centrosymmetric space group due to the absence of dipolar interactions in the ground state. Several octupolar molecules have been designed and tested for second order NLO response. Noteworthy among them are TATB,[5] crystal violet, tris(4-methoxyphenyl)cyclopropenylium bromide[7d] and triazene derivatives.[8]

Molecular systems like calixarenes, cryptands and macrocycles form an integral part of supramolecular chemistry and are important for their wide ranging applications in chemistry, biochemistry and materials research. Except for calixarenes,[9] however, these molecules remain mostly unexplored in the field of nonlinear optics. Only recently, a cyclophane derivative has been reported[10] where sterically constrained π–π stacking has been exploited for fine-tuning linear and NLO properties in the bulk. Besides, these molecules have an added advantage, as they can accommodate cations, anions or neutral molecules in their 3D cavity and thus provide the potential for tuning/switching the NLO property by supramolecular interactions inside the cavity.[11]

Cryptands having a three-fold symmetry axis passing through the two bridgehead atoms can act as perfect skeletons for designing bulk material for second order NLO. We have recently reported a cryptand in which three π–A chromophores have been attached resulting in a significant bulk second-order NLO response.[12] In the present work, we have used two different cryptand molecules $\mathbf{L_o}$ and $\mathbf{L_m}$ (the subscript o and m corresponds to *ortho* and *meta* substituted benzene units

†Electronic supplementary information (ESI) available: 400 MHz ^{1}H NMR spectra, 100 MHz ^{13}C NMR spectra, FAB-MS data of $\mathbf{L_1}$–$\mathbf{L_6}$, crystal structure packing diagrams for $\mathbf{L_1}$, $\mathbf{L_3}$ and $\mathbf{L_4}$. See http://www.rsc.org/suppdata/jm/b2/b202770b/

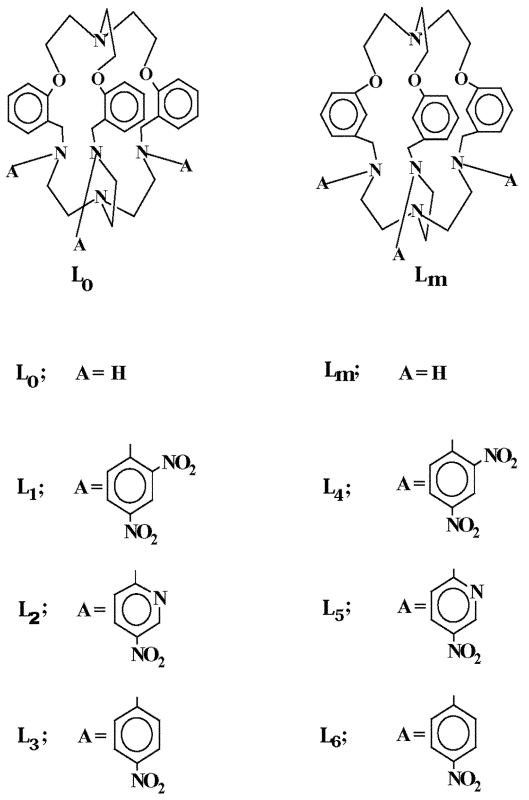

Fig. 1 Chemical structure of the cryptand headgroups ($\mathbf{L_o}$ and $\mathbf{L_m}$) and the D–π–A derivatives $\mathbf{L_1}$–$\mathbf{L_6}$.

present in the three bridges of the cryptands), which are the donor (D) units and derivatized them with three different π–A units to have D NLO chromophores with three-fold symmetry. The different π–A units incorporated in the cryptand strands are 2,4-dinitrobenzene, 5-nitropyridine and 4-nitrobenzene. These molecules have been used as efficient π–A units in important NLO molecules like methyl 2-(2,4-dinitroanilino)-propanoate (MAP),[13] 2-(*N*-prolinol)-5-nitropyridine (PNP)[14] and *N*-(4-nitrophenyl)-(L)-prolinol (NPP).[15] We have used two different cryptand cores of varying rigidity in order to see whether this effect gets reciprocated in their molecular and bulk NLO properties. The crystal structures of the compounds have been determined and their nonlinear optical properties at the microscopic as well as at the macroscopic levels explored. Fig. 1 displays the investigated structures. The N atoms in the three bridges of the cryptand act as the donor units. In $\mathbf{L_1}$, 2,4-dinitrobenzene is the π–A unit and one such unit is bonded to each nitrogen atom. In $\mathbf{L_2}$, the π–A unit has been replaced by 5-nitropyridine and in $\mathbf{L_3}$ by 4-nitrobenzene. Similarly, in $\mathbf{L_4}$, $\mathbf{L_5}$ and $\mathbf{L_6}$ the π–A units remain the same except the donor N-atoms are now organized in a different cryptand whose cavity is much more rigid due to the presence of *meta*-substituted benzene units.

Experimental section

o-N_5O_3 and *m*-N_5O_3 were synthesized as reported[16,17] earlier from our laboratory. Reagent grade 2,4-dinitrochlorobenzene (SD Fine Chem., India), 2-chloro-5-nitropyridine (Lancaster) and 1-fluoro-4-nitrobenzene (Fluka) were used without further purification. All the solvents were freshly distilled prior to use and all reactions were carried out under N_2 atmosphere.

Synthesis of the D–π–A molecules

The D–π–A substituted cryptands were synthesised by derivatizing the three secondary nitrogen atoms of the cryptand

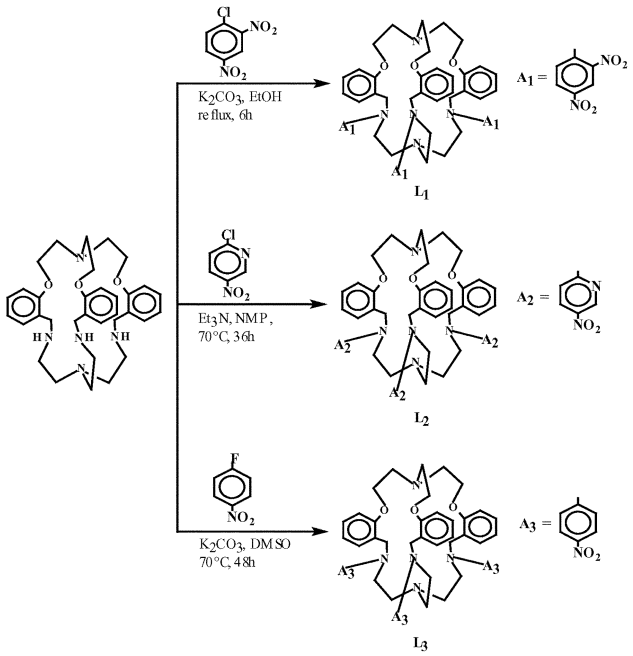

Scheme 1 Synthetic scheme for the compounds $\mathbf{L_1}$–$\mathbf{L_3}$.

(Scheme 1). The nitrogen atoms give the cryptand its donor (D) character and the π–A units were grafted by simple aromatic nucleophilic substitution (ArSN) reactions.[18] We systematically explore the different reaction conditions required for substituting the different π–A units.

^{1}H NMR and ^{13}C NMR spectra were recorded on a JEOL JNM-LA400 FT (400 and 100 MHz respectively) instrument in $CDCl_3$ with Me_4Si as the internal standard. FAB mass (positive ion) data were recorded on a JEOL SX 102/DA-6000 mass spectrometer using argon as the FAB gas at 6 kV and 10 mA with an accelerating voltage of 10 kV and the spectra were recorded at 298 K. Melting points were determined with an electrical melting point apparatus by PERFIT, India and were uncorrected. UV-visible spectra were recorded on a JASCO V-570 spectrophotometer in $CHCl_3$ at 298 K. Analytical data were obtained either from the microanalysis laboratory at IIT Kanpur or from the Central Drug Research Institute, Lucknow, India.

Synthesis

$\mathbf{L_1}$. To a solution of the *o*-cryptand $\mathbf{L_o}$ (0.56 g, 1 mmol) in dry EtOH (20 mL) was added anhydrous K_2CO_3 (0.44 g, 3.2 mmol) and the reaction mixture was stirred for 10 min. Subsequently, a solution of 2,4-dinitrochlorobenzene (0.65 g, 3.2 mmol) in dry EtOH (20 mL) was added dropwise in 30 minutes and the reaction mixture was allowed to reflux for 6 h. After cooling to RT, the solvent was removed under reduced pressure. The solid product obtained was repeatedly washed with water (6 × 200 mL). The tri-substituted product was purified by recrystallization from MeCN to give a yellow crystalline solid. Yield 92%; mp 215 °C; ^{1}H NMR: δ 2.27 (t, J = 6.2 Hz, 6H), 2.80 (t, J = 6.2 Hz, 6H), 3.11 (t, J = 4.3 Hz, 6H), 4.13 (t, J = 4.3 Hz, 6H), 4.37 (s, 6H), 6.61 (d, J = 9.6 Hz, 3H), 6.71–6.98 (m, 12H), 7.93 (dd, J = 9.6 Hz, J = 2.7 Hz, 3H), 8.51 (s, 3H). ^{13}C NMR: 50.44, 51.52, 52.60, 55.34, 66.68, 111.16, 118.09, 121.13, 122.94, 123.69, 127.44, 129.10, 129.45, 137.01, 137.15, 148.16, and 156.42 ppm. FAB-MS (*m*/*z*) 1058 (100%); Anal. calcd. for $C_{51}H_{51}N_{11}O_{15}$: C, 57.89; H, 4.86; N, 14.56. Found: C, 57.98; H, 4.97; N, 14.49%.

$\mathbf{L_2}$. To a solution of *o*-cryptand $\mathbf{L_o}$ (0.56 g, 1 mmol) in 20 mL of dry *N*-methyl-2-pyrrolidone (NMP) was added freshly

distilled Et_3N (0.32 g, 3.2 mmol). Subsequently, a solution of 2-chloro-5-nitropyridine (0.51 g, 3.2 mmol) in dry NMP (20 mL) was added dropwise in 45 minutes and the reaction mixture was allowed to stir at 70 °C for 36 h. It was then poured into cold water (250 mL). The pale yellow solid separated was collected by filtration and washed repeatedly with water (5 × 100 mL). The product was purified by recrystallization from acetone which afforded a brownish–red crystalline solid. Yield 91%; mp 220 °C; ^{1}H NMR: δ 2.87 (s br, 6H) 3.08 (s br, 6H), 3.79 (s br, 6H), 4.28 (s br, 6H), 4.82 (s, 6H), 6.12 (m, 3H), 6.66–7.15 (m, 12H), 7.62 (s br, 3H), 8.82 (s, 3H). ^{13}C NMR 49.11, 49.89, 50.90, 54.83, 63.83, 105.06, 111.47, 121.20, 124.26, 125.49, 128.46, 131.93, 134.70, 145.92, 155.56, and 159.87 ppm. FAB-MS (*m*/*z*) 926 (60%); Anal. calcd. for $C_{48}H_{51}N_{11}O_9$: C, 62.26; H, 5.55; N, 16.64. Found: C, 62.39; H, 5.68; N, 16.51%.

L_3. To a solution of *ortho*-cryptand **L_o** (0.56 g, 1 mmol) in dry DMSO (15 mL) was added anhydrous K_2CO_3 (0.44 g, 3.2 mmol). Subsequently 1-fluoro-4-nitrobenzene (0.45 g, 3.2 mmol) in dry DMSO (15 mL) was added dropwise in 30 minutes and the reaction mixture was allowed to stir at 70 °C for 48 h. The reaction mixture was then poured into cold water (250 mL). The yellow solid separated was collected by filtration and was washed thoroughly with water (5 × 100 mL). The tri-substituted product was purified by column chromatography (SiO_2 100–200 mesh, hexane–EtOAc 4 : 1) and recrystallized from MeCN to obtain a bright yellow crystalline solid. Yield 92%; mp 230 °C; ^{1}H NMR: δ 2.78 (s br, 6H), 3.07 (s br, 6H), 3.56 (s br, 6H), 4.29 (s br, 6H), 4.85 (s, 6H), 6.44 (d, J = 9.3 Hz, 6H), 6.53–7.23 (m, 12H), 7.74 (d, J = 9.3 Hz, 6H). ^{13}C NMR: 50.22, 51.12, 51.25, 53.79, 63.96, 110.20, 111.45, 120.88, 124.54, 125.46, 125.86, 128.19, 136.89, 151.49, and 155.69 ppm. FAB-MS (*m*/*z*) 923 (70%); Anal. calcd. for $C_{51}H_{54}N_8O_9$: C, 66.36; H, 5.89; N, 12.14. Found: C, 66.39; H, 5.97; N, 12.01%.

L_4. A procedure similar to that adopted for **L_1** was followed, and the *meta*-cryptand **L_m** was used in place of **L_o**. Yield 90%; mp 160 °C; ^{1}H NMR: δ 2.48 (t, J = 6.2 Hz, 6H), 3.02 (t, J = 6.2 Hz, 6H), 3.19 (t, J = 4.4 Hz, 6H), 4.04 (t, J = 4.4 Hz, 6H), 4.20 (s, 6H), 6.60 (s, 3H), 6.72–6.77 (m, 9H), 7.23–7.26 (m, 3H), 8.09 (dd, J = 9.4 Hz, J = 2.7 Hz, 3H), 8.59 (d, J = 2.7 Hz, 3H). ^{13}C NMR: 51.12, 52.66, 56.10, 58.51, 69.25, 114.10, 114.27, 118.98, 119.46, 123.30, 127.79, 130.01, 136.78, 138.12, 138.23, 148.28, and 160.11 ppm. FAB-MS (*m*/*z*) 1058 (100%); Anal. calcd. for $C_{51}H_{51}N_{11}O_{15}$: C, 57.89; H, 4.86; N, 14.56. Found: C, 57.84; H, 4.93; N, 14.43%.

L_5. A procedure similar to that adopted for **L_2** was followed using **L_m** in place of **L_o**. Yield 90%; mp 130 °C; ^{1}H NMR: δ 2.65 (t, J = 6.2 Hz, 6H), 3.02 (t, J = 5.0 Hz, 6H), 3.61 (t, J = 6.2 Hz, 6H), 3.92 (t, J = 5.0 Hz, 6H), 4.67 (s, 6H), 6.32 (d, J = 9.5 Hz, 3H), 6.61–7.17 (m, 12H), 8.10 (dd, J = 9.5 Hz, J = 2.7 Hz, 3H), 8.97 (d, J = 2.7 Hz, 3H). ^{13}C NMR: 47.83, 52.88, 53.33, 56.87, 68.59, 104.82, 113.29, 114.32, 119.05, 129.94, 132.95, 135.28, 137.98, 146.42, 159.70, and 160.44 ppm. FAB-MS (*m*/*z*): 926 (50%); Anal. calcd. for $C_{48}H_{51}N_{11}O_9$; C, 62.26, H, 5.55, N, 16.64. Found: C, 62.40; H, 5.59; N, 16.48%.

L_6. This was synthesized using **L_m** following the method used for **L_3**. Yield 91%; mp 165 °C; ^{1}H NMR: δ 2.59 (t, J = 6.2 Hz, 6H), 3.06 (t, J = 4.6 Hz, 6H), 3.35 (t, J = 6.2 Hz, 6H), 3.97 (t, J = 4.6 Hz, 6H), 4.44 (s, 6H), 6.48 (d, J = 9.4 Hz, 6H), 6.56 (s, 3H), 6.66–7.18 (m, 9H), 8.03 (d, J = 9.4 Hz, 6H). ^{13}C NMR: 49.49, 53.07, 55.15, 57.10, 68.76, 110.79, 113.56, 114.06, 118.64, 126.28, 130.07, 137.66, 137.99, 152.93, and 159.89 ppm. FAB-MS (*m*/*z*) 923 (30%) Anal. calcd. for $C_{51}H_{54}N_8O_9$: C, 66.36; H, 5.89; N, 12.14. Found: C, 66.51; H, 5.94; N, 12.06%.

X-Ray crystallography. Single crystals could be grown by slow evaporation of the D–π–A cryptands at room temperature in pyridine in the case of **L_1** and MeCN in the cases of **L_3** and **L_4**. All our efforts to have single crystals of the remaining compounds suitable for X-ray crystallography remained unsuccessful. In each case, large triangular crystals (up to ~4 mm each side) could be isolated. For the X-ray crystallographic work, a suitable crystal of each compound was mounted at the end of a glass fiber with epoxy cement. Cell parameters and reflection intensities were measured at 298 K on an Enraf–Nonius CAD-4 Mach diffractometer with graphite-monochromated Mo K_α radiation (α = 0.71073 Å). The cell parameters were determined by least-squares fitting of 25 centered reflections in the range, $18 \leqslant 2\theta \leqslant 28$. The lattice parameters, data collection method, structure solution and refinement details are listed in Table 1. The structures of **L_3** and **L_4** were solved by the direct method using SIR92[19] and was

Table 1 Crystallographic data for the D–π–A cryptands **L_1**, **L_3** and **L_4**

	L_1	**L_3**	**L_4**
Empirical formula	(C51 H51 N11 O15) ·1/3 (C5 H5 N)	C53 H57 N9 O9	C53 H54 N12 O15
Formula weight	1084.40	964.08	1099.08
Temperature	293(2) K	293(2) K	293(2) K
Wavelength	0.71073 Å	0.71069 Å	0.71073 Å
Crystal system	Trigonal	Orthorhombic	Triclinic
Space group	*P*3	*Pbca*	$P\bar{1}$
a	16.63(5)	12.473(4) Å	11.798(2) Å
b	16.63(6)	21.974(5) Å	12.137(7) Å
c	16.00(3)	36.982(17) Å	19.707(6) Å
α	90.00°	90.00°	89.51(6)°
β	90.00°	90.00°	79.11(2)°
γ	120.00°	90.00°	75.62(4)°
Volume	3832(14) Å^3	10136(6) Å^3	2682.0(19) Å^3
Z	3	8	2
Density (calculated)	1.431 Mg m^{-3}	1.26 Mg m^{-3}	1.361 Mg m^{-3}
F(000)	1704	4080	1152
Crystal size	0.18 × 0.2 × 0.2 mm^3	0.2 × 0.2 × 0.2 mm^3	0.3 × 0.2 × 0.2 mm^3
Independent Reflections	3753	6604	7396
Goodness-of-fit	2.321	1.016	0.935
Final *R* indices	*R*1 = 0.066	*R*1 = 0.069	*R*1 = 0.084
[$I > 2\sigma(I)$]	*wR*2 = 0.065	*wR*2 = 0.154	*wR*2 = 0.223
R indices (all data)	*R*1 = 0.113	*R*1 = 0.286	*R*1 = 0.310
	*wR*2 = 0.109	*wR*2 = 0.211	*wR*2 = 0.342
Refinement method	Full-matrix least- squares on *F*	Full-matrix least- squares on F^2	Full matrix least- squares on F^2

refined on F^2 by full-matrix least-squares technique using the SHELXL-97[20] program package. For $\mathbf{L_1}$, the structure was solved by the direct method and refined on F by full-matrix least-squares techniques using XTAL 3.2 program package.[21] Both $\mathbf{L_1}$ and $\mathbf{L_4}$ crystals diffracted weakly. So, in case of $\mathbf{L_1}$, only the N and O atoms were refined anisotropically while for $\mathbf{L_4}$, the N, O and the benzene C atoms were refined anisotropically. For all the three structures, the H atoms were not refined but included in the final structure factor calculations. CCDC 172621–172623. See http://www.rsc.org/suppdata/jm/b2/b202770b/ for crystallographic files in .cif or other electronic format.

NLO measurements. Second harmonic measurements in solution were carried out by the HRS technique. In HRS experiments, the fundamental (1064 nm) of a Q-switched Nd : YAG laser (Spectra Physics, DCR-3G, 8 ns) beam was focused by a biconvex lens (f.l. 10 cm) to a spot 5 cm away after passing through the glass cell containing the sample. The scattered light in the perpendicular direction was collected by a UV-Visible sensitive photomultiplier tube (PMT). A monochromator (Czerny Turner 0.25 m) was used for wavelength discrimination and no other collection optics were employed. The input power was monitored using a power meter. All data were collected at laser powers $\leqslant 24$ mJ pulse^{-1} which is below the threshold for stimulated Raman, self-focusing/self-defocusing, Brillouin scattering and dielectric breakdown. The experimental set-up was first standardized by measuring the β value for pNA in $CHCl_3$ by the external reference method[22a] and a value of 18×10^{-30} esu was obtained which was close to the reported value for this compound.[21b] The monochromator was scanned at intervals of 2 nm to find if the signal at the second harmonic wavelength has any contribution from two photon fluorescence of $\mathbf{L_1}$–$\mathbf{L_6}$. In fact, it was found that these molecules do not have any two photon fluorescence around 532 nm. Fig. 2 displays a plot of $I_{2\omega}/I_{\omega}^2$ *vs.* number density of $\mathbf{L_3}$ as well as the reference pNA. From the ratio of the two slopes in Fig. 2 the β value of $\mathbf{L_3}$ was determined by the external reference method. Similarly β for other cryptands was obtained.

The powder SHG measurements were carried out using the Kurtz–Perry method[23] using the fundamental (1064 nm) of a Q-switched Nd : YAG laser (Spectra Physics, DCR-11, 8 ns). The beam was split into two by a beam splitter and the reflected beam passed through the powder sample. The transmitted beam through the sample contained both the fundamental and second harmonic wavelengths. The fundamental was removed first by a saturated $CuSO_4$ solution in water and a broad band IR filter (BG 38). The signal then passed through an interference filter (532 nm, 4 nm bandwidth) and was detected by a photodiode. Urea was used for calibrating the SHG signal. The

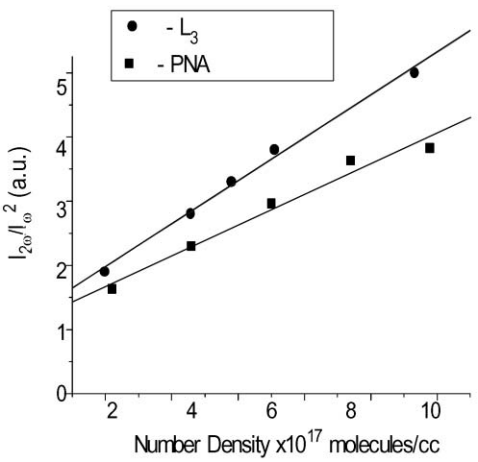

Fig. 2 A plot of $I_{2\omega}/I_{\omega}^2$ *vs.* number density of $\mathbf{L_3}$ as well as ref. pNA.

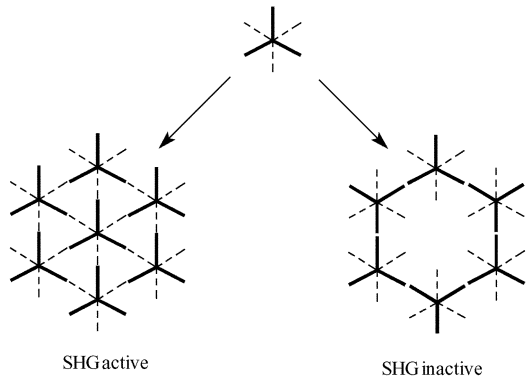

Fig. 3 View of a centrosymmetric hexagonal lattice and a non-centrosymmetric trigonal lattice.

compounds showed excellent stability under laser irradiation and no sign of decomposition could be detected.

Results and discussion

Molecular and crystal structures

As the cryptand core inherits a 3-fold axis of symmetry, there arises two possible pathways (Fig. 3) by which these molecules can crystallize: a planar centrosymmetric hexagonal lattice formed by the interactions between identical groups resulting in SHG inactive molecules or a non-centrosymmetric trigonal lattice formed by the interaction between different groups showing SHG activity. Single crystals of $\mathbf{L_1}$ adopt a trigonal space group while $\mathbf{L_3}$ and $\mathbf{L_4}$ crystallize in orthorhombic and triclinic space groups, respectively. All of the three crystal structures maintain the molecular 3-fold axis of symmetry passing through the bridgehead N atoms. Both the ^1H and ^{13}C NMR data are consistent with a 3-fold symmetry of these molecules.

$\mathbf{L_1}$. This tris D–π–A cryptand crystallizes[12] in a unique non-centrosymmetric trigonal space group $P3$. In the asymmetric unit cell, three strands are present and they generate a triad involving A, B and C molecules with the C_3 symmetry axis passing through the centre of the triad (Fig. 4). The bridgehead nitrogens maintain an *endo–endo* conformation. The molecule A has a remarkably short distance 4.588(8) Å between the bridgehead N atoms, while the same in molecules B and C are

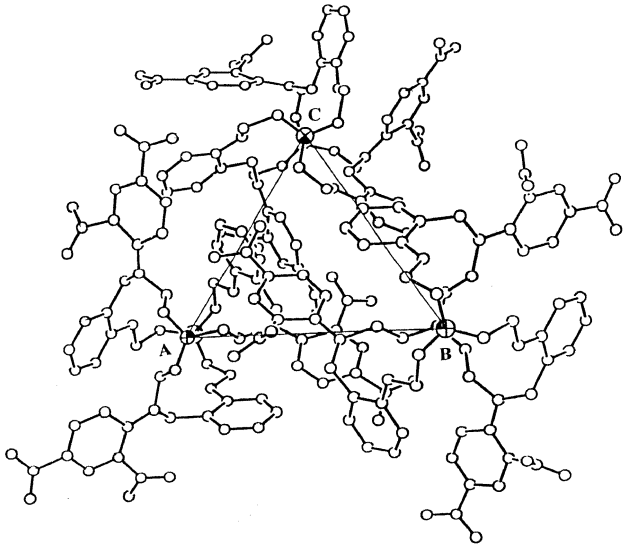

Fig. 4 View of a perfect trigonal network formed by the molecules **A**, **B** and **C** with the C_3 axis passing through the center of the triad.

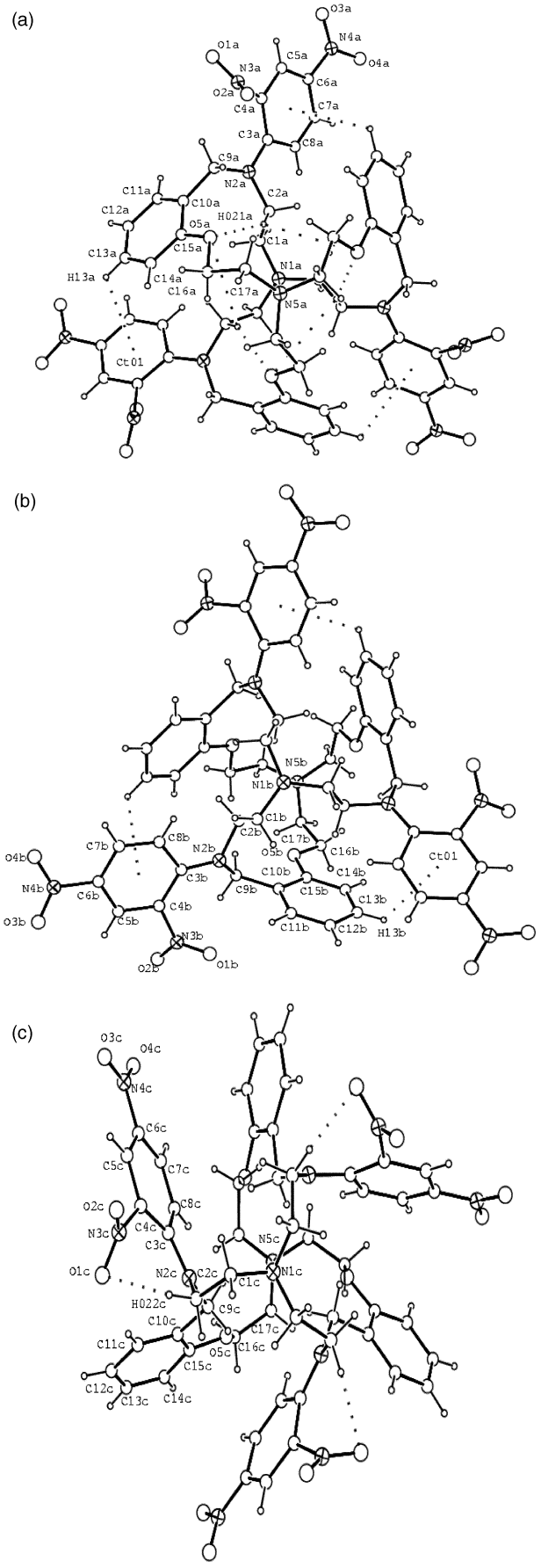

Fig. 5 (a) A perspective view of molecule **A** down the *c*-axis showing different intramolecular interactions. (b) A view of the molecule **B** down the *c*-axis showing intramolecular interactions. (c) A view of the molecule **C** down the *c*-axis showing intramolecular interactions.

6.672(12) Å and 6.384(12) Å, respectively. Thus, while in A, the bridgehead nitrogens are pushed inward significantly, they are pushed outward slightly compared to the underivatized cryptand $\mathbf{L_o}$ (6.249 Å).[24] This shows that the parent cryptand is quite flexible which is not unprecedented for these type of molecules.[25a] The average distance of the N(amino)–C(benzene) bond is 1.376 Å which is considerably shorter than C–N single bond distance of ~1.45 Å confirming that the amino nitrogen of the cryptand moiety is conjugated with the aromatic ring of the acceptor. The other bond distances and angles in $\mathbf{L_1}$ are within normal literature values.[13,24] The intramolecular interactions vary in the D–π–A cryptand molecules A, B and C.

Molecule **A** exhibits two kinds of weak intramolecular H-bonding interactions (Fig. 5a): (i) a C–H···O hydrogen bond involving the C atom (C2a), the H atom (H021a) and the O (O5a) of the phenyl ring with a C–O distance of 3.244 Å. (ii) a C–H···π interaction involving C atom (C13a) of the phenyl ring, H atom (H13a) and the centroid of the dinitro substituted phenyl ring (Ct01) of the symmetry related strand with a C–π distance of 3.850 Å.

Molecule **B** shows a C–H···π interaction similar to that observed in molecule **A** (Fig. 5b). It involves the C atom (C13b) of the phenyl ring, H atom (H13b) and the centroid of the dinitro substituted benzene ring (Ct01) of the symmetry related strand with a C–π distance of 3.916 Å.

Molecule **C** shows an intramolecular C–H···O interaction (Fig. 5c) involving C atom (C2c), H atom (H022c) and O atom (O1c) of the *ortho*-nitro group with a C–O distance of 2.978 Å. The phenyl and the dinitro substituted benzene rings are far apart and thus are not involved in the C–H···π interactions found in molecules **A** and **B**.

It is to be noted that only $\frac{1}{3}$ of each molecule **A**, **B** and **C** are in the asymmetric unit. In effect, therefore, the molecule **A** has six intramolecular (three C–H···O and three C–H···π) interactions, molecule **B** has three C–H···π interactions, while molecule **C** shows three intramolecular C–H···O interactions. These interaction distances are collected in Table 2.

Two different kinds of intermolecular H-bonding interactions are present amongst **A**, **B** and **C** leading to the trigonal network. Molecules **A** and **B** are held together by one C–H···O interaction involving C atom (C8b) of the dinitro substituted benzene ring, H atom (H08b) of the molecule **B** and O atom (O3a) of the nitro group of molecule **A** having a C–O distance of 3.279 Å (Fig. 6). Likewise, molecules **B** and **C** interact by forming another C–H···O hydrogen bond involving benzylic carbon (C9b), H atom (H091b) and oxygen atom (O4c) of the nitro group with a C–O distance of 3.285 Å. Molecules **B** and **C** also interact in an edge-to-face manner forming a C–H···π bond with a distance of 3.583 Å. These distances for the intermolecular interactions are also given in Table 2.

$\mathbf{L_3}$. This molecule crystallizes in the orthorhombic space group *Pbca*. A perspective view of the molecule is shown in (Fig. 7). Like in the case of **A**, **B** and **C** molecules in $\mathbf{L_1}$, this

Table 2 Geometrical parameters for various interactions in the molecules **A**, **B** and **C** of $\mathbf{L_1}$

Molecule	Interaction (Intra)	*D*/Å	*d*/Å	*θ*/deg
A	C(2a)–H(021a)···O(5a)	3.244	2.395	148.57
	C(13a)–H(13a)···Ct(01)	3.850	3.363	115.02
B	C(13b)–H(13b)···Ct(01)	3.916	3.432	114.98
C	C(2c)–H(022c)···O(1c)	2.978	2.195	138.97
(Inter)				
A, **B** and **C**	C(8b)–H(08b)···O(3a)	3.279	2.540	134.84
	C(9b)–H(091b)···O(4c)	3.285	2.568	132.45
	C(13b)–H(13b)···Ct(01)	3.583	3.000	122.26

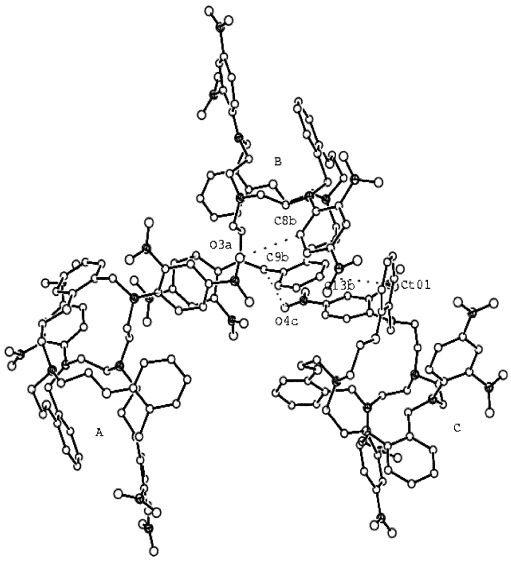

Fig. 6 A perspective view of the molecules **A**, **B** and **C** showing the intermolecular interactions. H atoms and solvent molecules have been removed for clarity.

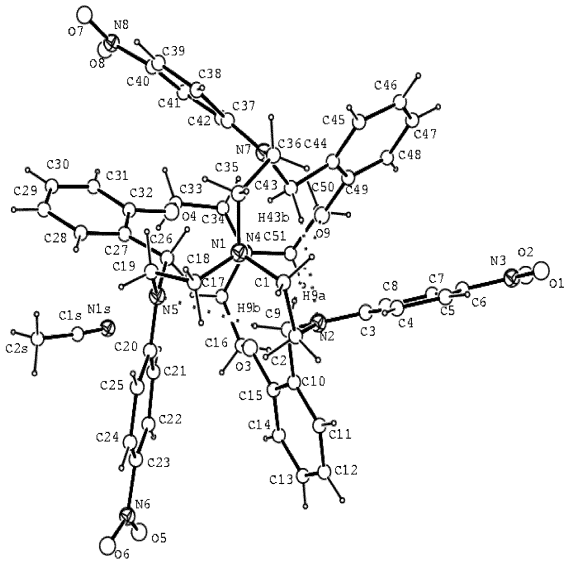

Fig. 7 View of $\mathbf{L_3}$ down the *c*-axis showing the intramolecular interactions.

D–π–A cryptand maintains an *endo–endo* conformation with a distance of 6.587 Å between the bridgehead N atoms which is slightly longer than that of $\mathbf{L_o}$. All the bond distances and angles are within normal literature values.[15,24]

The intramolecular interactions in this D–π–A cryptand involve two C–H···N and one C–H···O bond across the 3D cavity of the cryptand (Fig. 7). One of the C–H···N hydrogen bonds is formed between the C atom (C9) of the benzylic amino group, H atom (H9b) and amino N atom (N5) with a C–N distance of 3.890 Å. The second C–H···N hydrogen bonding interaction involves the atoms C43, H43b, and N2, with a C–N distance of 3.563 Å. The C–H···O hydrogen bond is formed between the C atom (C9) of the benzylic amino group, H atom (H9a) and oxygen atom (O9) of the phenyl ring with a distance of 3.871 Å. The intramolecular distances are listed in Table 3. This molecule does not show any significant intermolecular interactions in the crystal lattice.

$\mathbf{L_4}$. The structure of this molecule could be solved in both the triclinic space groups, *P*1 and $P\bar{1}$. However, in the non-centrosymmetric space group *P*1, the structure did not refine well and many N and O atoms gave negative temperature factors when refined anisotropically. In spite of the fact that this molecule is SHG active, we could refine the structure well in the triclinic centrosymmetric space group. An *endo–endo* conformation is maintained by this molecule as well with a distance of 8.656(11) Å between the bridgehead N atoms (Fig. 8) which is significantly shorter compared to that in $\mathbf{L_m}$ (9.904 Å).[17] All the bond distances and angles are within normal literature values.[13,25*b*]

The intramolecular interactions in $\mathbf{L_4}$ involve one C–H···O and one C–H···N bond (Fig. 8). The benzylic C atom (C26) acts as the H-bond donor while the bridgehead tertiary N atom (N1) acts as the H-bond acceptor with a C–N distance of 3.165 Å. The C–H···O hydrogen bond is formed between C atom (C18) which is the H-bond donor and O atom of the nitro group (O6) which acts as the H-bond acceptor with a C–O distance of 3.128 Å. The intramolecular H-bond distances are listed in Table 3.

There are three C–H···O intermolecular hydrogen bonding interactions between the neighbouring molecules in the crystal lattice (Fig. 9). The carbon atom (C5) acts as a strong H bond donor as it is placed between two nitro groups. Thus C5 and

Table 3 Geometrical parameters for various interactions in the structure $\mathbf{L_3}$ and $\mathbf{L_4}$

Molecule	Interaction (Intra)	*D*/Å	*d*/Å	θ/deg
$\mathbf{L_3}$	C(9)–H(9b)···N(5)	3.890	2.929	170.69
	C(43)–H(43b)···N(2)	3.563	2.629	161.84
	C(9)–H(9a)···O(9)	3.871	2.907	173.15
$\mathbf{L_4}$	C(26)–H(261)···N(1)	3.165	2.419	136.89
	C(26) –H(26a)···N(1)	3.180	2.431	134.00
	C(18)–H(182)···O(6)	3.128	2.413	131.87
	C(18)–H(18a)···O(6) (Inter)	3.180	2.447	132.11
$\mathbf{L_4}$	C(5)–H(05)···O(13)	3.409	2.539	153.88
	C(5)–H(5)···O(13)	3.400	2.507	161.44
	C(43)–H(431)···O(12)	3.408	2.583	148.58
	C(43)–H(43b)···O(12)	3.430	2.572	148.18

D is the distance between C and the acceptor (O, N, or ring centroid); *d* is the distance between H and the acceptor (O, N, or ring centroid); θ is the angle at H in C–H···A (A=O, N, or ring centroid); Ct is the centroid of the aromatic ring acting as the C–H acceptor; For π···π interactions, D is the perpendicular stacking distance.

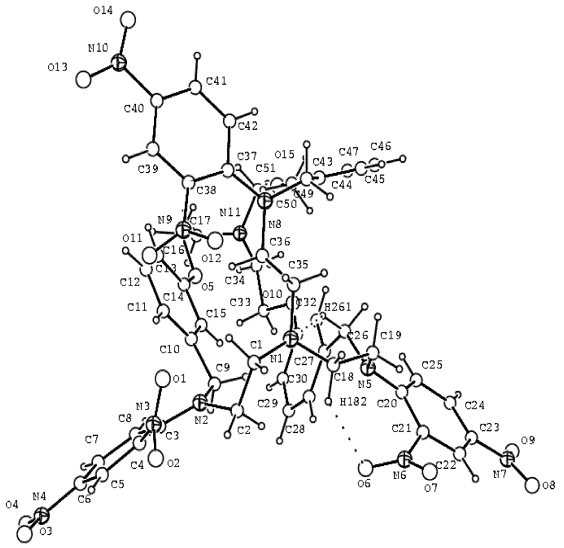

Fig. 8 A perspective view of $\mathbf{L_4}$ and the intramolecular interactions shown by dashed lines.

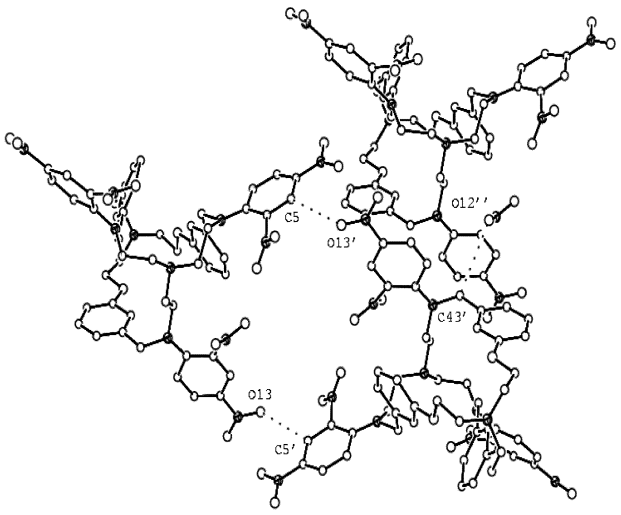

Fig. 9 View of the molecules in $\mathbf{L_4}$ and various intermolecular interactions present shown by dashed lines. H atoms and solvent molecules have been removed for clarity.

C5′ form two C–H···O hydrogen bonds with the oxygen atoms O13′ and O13 respectively with a C–O distance of 3.409 Å. The third C–H···O hydrogen bond is formed by the interaction of the benzylic carbon (C43′) and the oxygen of the nitro group (O12″) of the neighbouring molecule with a C–O distance of 3.408 Å. These interaction distances are collected in Table 3.

Linear and nonlinear optical properties

The UV-visible spectral data of compounds $\mathbf{L_1}$–$\mathbf{L_6}$ were recorded in $CHCl_3$ and are displayed in Fig. 10. All the spectra are characterized by an intense charge-transfer absorption in the near ultraviolet. The molecules $\mathbf{L_1}$, $\mathbf{L_2}$ and $\mathbf{L_3}$ have their charge-transfer band red-shifted by 6–10 nm and are more intense compared to $\mathbf{L_4}$, $\mathbf{L_5}$ and $\mathbf{L_6}$. This can be explained by the increase of the inductive donor effect of the *ortho*-cryptand in comparison to the *meta*-cryptand. Thus, the D–π–A *meta*-cryptands offer a better transparency compared to the corresponding *ortho* D–π–A cryptands.

The first hyperpolarizabilities, β of $\mathbf{L_1}$–$\mathbf{L_6}$ were measured by hyper-Rayleigh scattering[26] in $CHCl_3$ and the β values of the D–π–A cryptands, $\mathbf{L_1}$–$\mathbf{L_6}$, are given in Table 4. The corresponding β_0 static values were derived from the well-known two-state model[27] and are listed as well. The nonlinearity of $\mathbf{L_1}$ and $\mathbf{L_2}$ are comparable to the classical well-known *para*-nitroaniline (pNA) molecule, with $\beta_0 = 10 \times 10^{-30}$ esu as

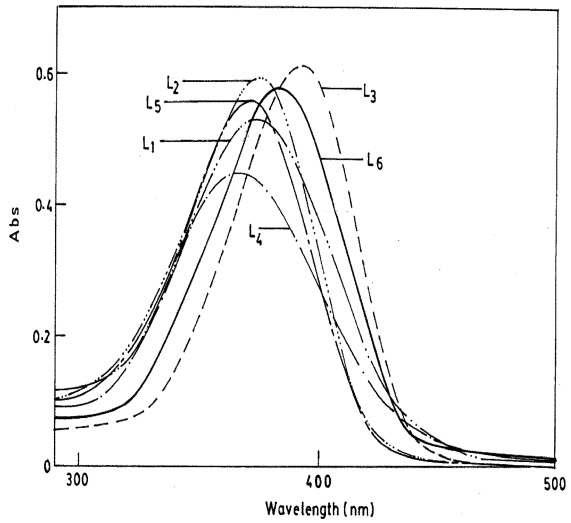

Fig. 10 UV spectra of $\mathbf{L_1}$–$\mathbf{L_6}$ (1×10^{-5} M) in $CHCl_3$.

Table 4 Results of hyper-Rayleigh scattering measurements on compounds $\mathbf{L_1}$–$\mathbf{L_6}$ at 1064 nm

	pNA	$\mathbf{L_1}$	$\mathbf{L_2}$	$\mathbf{L_3}$	$\mathbf{L_4}$	$\mathbf{L_5}$	$\mathbf{L_6}$
λ_{max}	347	370	376	390	364	368	380
$\beta \times 10^{-30}$ esu	18.0	16	16.1	19.0	20	22	27
$\beta_0 \times 10^{-30}$ esu	10	10.6	10.5	12.2	14	15	18

measured in $CHCl_3$, whereas, $\mathbf{L_3}$ has a slightly higher value (1.2 times) with respect to pNA. The results for the D–π–A *meta*-cryptand derivatives are interesting in a number of ways. The second order polarizability is greater than that of pNA or *ortho*-cryptands. In addition, in *meta*-cryptand $\mathbf{L_4}$, the charge-transfer band is blue-shifted compared to the D–π–A *ortho*-cryptand, $\mathbf{L_1}$ leading to a greater transparency. Moreover, the second order polarizability also increases. Similarly, $\mathbf{L_5}$ has a higher β compared to the corresponding *ortho*i D–π–A cryptand *i.e.* $\mathbf{L_2}$ and better transparency. $\mathbf{L_6}$ has the highest β value in the series and the corresponding static hyperpolarizability value is almost double that of the classical pNA molecule.

The greater transparency as well as hyperpolarizability of the group $\mathbf{L_4}$–$\mathbf{L_6}$ compared to $\mathbf{L_1}$–$\mathbf{L_3}$ could be attributed to greater rigidity of the $\mathbf{L_m}$ framework compared to that of $\mathbf{L_o}$ as seen from the molecular conformation in the solid state. The relatively high β value obtained for $\mathbf{L_6}$ while maintaining an excellent transparency in the visible range points out its particular relevance in NLO applications. Thus, a favourable orientation of these chromophores across the cryptand core can be effectively utilized for designing such systems with a large SHG response, although the C_3 symmetric chromophore subunits remain unconjugated.

Powder second-harmonic generation (SHG) measurements were carried out on X-ray crystallographically characterized $\mathbf{L_1}$, $\mathbf{L_3}$ and $\mathbf{L_4}$ in order to evaluate their potential as second order NLO materials. Compound $\mathbf{L_1}$ exhibited a SHG powder signal which was 0.6 times that of urea in conformity with its acentric crystallization. Powder samples of $\mathbf{L_2}$ also showed a SHG signal of 1.0 times that of urea. These efficiencies are certainly better than those reported for the triaryloxy triazines by Thalladi *et al.*[8b] where similar H-bonding and stacking interactions are operational to stabilise the three-dimensional structures.

It is important to note that $\mathbf{L_3}$ in spite of being crystallized in a centrosymmetric space group, shows an SHG powder signal efficiency of 0.05 times that of urea. This points to the presence of some defect sites in the crystal. Although the molecules crystallize in a centrosymmetric space group, there may be regions or zones having defects. In fact, such defects are known in organic molecules and they play a major role in determining the outcome of a photochemical dimerization reaction in the solid state.[28] In fact, the X-ray crystallographic data pertaining to the macroscopic ordered region of the crystal say nothing about the molecular packing in the defect region. $\mathbf{L_3}$ is stabilized by the H-bonding and stacking interactions in a different fashion compared to the other two cases. This perhaps, would explain why it adopted a centrosymmetric packing. Further experiments are necessary to determine the exact nature of the defects in $\mathbf{L_3}$. Compound $\mathbf{L_4}$ also shows a SHG powder signal of 0.36 times that of urea although it crystallizes in a centrosymmetric $P\bar{1}$ space group. This could be as a result of polymorphism of the crystalline structure or due to a slight difference in the respective molecular orientations within the structural unit cell with respect to a fully centrosymmetric case. This result is not unprecedented and was earlier observed in the case of TATB which also crystallizes in a $P\bar{1}$ space group and shows substantial SHG activity.[5,6b] Electron diffraction experiments on TATB indicate[6a] that the structural modulation on the *c*-axis gives rise to the resultant SHG value. Similar

electron diffraction studies on $\mathbf{L_4}$ can throw light on the origin of the observed SHG value but that will be another study.

Conclusion

We have shown that bulk second harmonic materials can be built around the three-fold symmetry of cryptand molecules, with strikingly high melting points, exploiting weak molecular forces. However, intermolecular interaction is necessary for a non-centrosymmetric packing in the crystal. The search for an optimal transparency–efficiency trade-off for optically non-linear molecules has led to different approaches *via* molecular engineering. Cryptand molecules with their inherent three-fold symmetry and three secondary nitrogen atoms are ideal for further derivatization which can provide an easy way to engineer new molecular systems for NLO molecules and materials. Besides, the cavity of a cryptand can be tailored to accept a metal ion which can offer possibilities for tuning/switching capabilities in NLO materials. Research along these lines is in progress in our laboratory.

Acknowledgement

This work was supported by the Department of Science and Technology, New Delhi, India (Grant No. SP/S1/F-08/96 to PKB). We would also like to thank the CSIR, Govt. of India for funding this research. We are grateful to K. Venkatesan for many enlightening discussions.

References

1 (*a*) D. S. Chemla and J. Zyss, *Nonlinear Optical Properties of Organic Molecules and Crystals*, Academic Press, Boston, 1987; (*b*) J. Zyss, *Molecular Nonlinear Optics: Materials, Physics and Devices*, Academic Press, Boston; (*c*) P. N. Prasad and D. J. Williams, *Introduction to Nonlinear Optical Effects in Molecules and Polymers*, John Wiley and Sons, New York, 1991.
2 (*a*) J.-L. Oudar and D. S. Chemla, *J. Chem. Phys.*, 1977, **66**, 2664; (*b*) J.-L. Oudar, *J. Chem. Phys.*, 1977, **67**, 446; (*c*) R. Wortman, P. Kramer, C. Glania, S. Lebus and N. Detzer, *Chem.Phys.*, 1993, **173**, 99; (*d*) S. R. Marder, L.-T. Cheng and B. G. Tiemann, *J. Chem. Soc., Chem. Commun.*, 1992, 672.
3 L.-T. Cheng, W. Tam, S. H. Stevenson, G. R. Meredith, G. Rikken and S. R. Marder, *J. Phys. Chem.*, 1991, **95**, 10631.
4 J. Zyss, *Nonlinear Opt.*, 1991, **1**, 3.
5 I. Ledoux, J. Zyss, J. Siegel, J. Brienne and J.-M. Lehn, *Chem. Phys. Lett.*, 1990, **172**, 440.
6 (*a*) I. G. Voigt-Martin, Gao. Li, A. Yakimanski, G. Schulz and J. J. Wolff, *J. Am. Chem. Soc.*, 1996, **118**, 12831; (*b*) G. Filippini and A. Gavezzoti, *Chem. Phys. Lett.*, 1994, **231**, 86.
7 (*a*) M. Joffre, D. Yaron, R. J. Silbey and J. Zyss, *J. Chem. Phys.*, 1992, **97**, 5607; (*b*) J. L. Bredas, F. Meyers, B. M. Pierce and J. Zyss, *J. Am. Chem. Soc.*, 1992, **114**, 4928; (*c*) J. Zyss, Y. C. Van, C. Dhenaut and I. Ledoux, *Chem.Phys.*, 1993, **177**, 281; (*d*) T. Verbiest, K. Clays, C. Samien, J. J. Wolff, D. Reinhoudt and A. Persoons, *J. Am. Chem. Soc.*, 1994, **116**, 9320; (*e*) S. Stadler, F. Feiner, C. Brauchle, S. Brandl and R. Gompper, *Chem. Phys. Lett.*, 1995, **245**, 292; (*f*) R. Wortmann, C. Glania, P. Kramer, R. Matschiner, J. J. Wolff, S. Craft, B. Treptow, E. Barbu, D. Langle and G. Gorlitz, *Chem.-Eur. J.*, 1997, **3**, 1765.
8 (*a*) P. C. Ray and P. K. Das, *Chem. Phys. Lett.*, 1995, **244**, 153; (*b*) V. R. Thalladi, S. Brasselet, H.-C. Weiss, D. Blaser, A. K. Katz, H. L. Carrell, R. Boese, J. Zyss, A. Nangia and G. R. Desiraju, *J. Am. Chem. Soc.*, 1998, **120**, 2563; (*c*) V. R. Thalladi, R. Boese, S. Brasselet, I. Ledoux, J. Zyss, R. K. R. Jetti and G. R. Desiraju, *Chem. Commun.*, 1999, 1639.
9 E. Kelderman, L. Derhaeg, G. J. T. Heesink, W. Verboom, J. F. J. Engbersen, N. F. V. Hulst, A. Persoons and D. N. Reinhout, *Angew. Chem., Int. Ed. Engl.*, 1992, **31**, 1075.
10 J. Zyss, I. Ledoux, S. Volkov, V. Chernyak, S. Mukamel, G. P. Bartholomew and G. C. Bazan, *J. Am. Chem. Soc.*, 2000, **122**, 11956.
11 S. Houbrechts, Y. Kubo, T. Tozawa, S. Tokita, T. Wada and H. Sasabe, *Angew. Chem., Int. Ed. Engl.*, 2000, **39**, 3859.
12 P. Mukhopadhyay, P. K. Bharadwaj, G. Savitha, A. Krishnan and P. K. Das, *Chem. Commun.*, 2000, 1815.
13 J.-L. Oudar and R. Hierle, *J. Appl. Phys.*, 1997, **48**, 2699.
14 R. J. Tweig and C. W. Dirk, *J. Chem. Phys.*, 1986, **85**, 3537.
15 J. Zyss, J. F. Nicoud and M. Coquillay, *J. Chem. Phys.*, 1984, **81**, 4160.
16 P. Ghosh, P. K. Bharadwaj, S. Mandal and S. Ghosh, *J. Am. Chem. Soc.*, 1996, **118**, 1553.
17 D. K. Chand and P. K. Bharadwaj, *Inorg. Chem.*, 1996, **35**, 3380.
18 (*a*) R. E. Parker, *Adv. Fluorine Chem.*, 1963, **3**, 63; (*b*) H. E. Smith, W. I. Cozart, T. de Paulis and F. M. Chen, *J. Am. Chem. Soc.*, 1979, **101**, 5186.
19 A. Altomare, G. Cascarano, C. Giacovazzo and A. Gualardi, *J. Appl. Cryst.*, 1993, **26**, 343.
20 G. M. Sheldrick, SHELXL-97: Program for crystal structure refinement, University of Göttingen, Germany, 1997.
21 S. R. Hall, J. M. Stewart, H. B. Flack, *The XTAL 3.2 Reference Manual*, Universities of Western Australia and Maryland: Nedlands, Australia, and College Park, MD, USA, 1993.
22 (*a*) T. Kodaira, A. Watanabe, O. Ito, M. Matsuda, K. Clays and A. Persoons, *J. Chem Soc., Faraday Trans.*, 1997, **93**, 3039; (*b*) P. C. Ray and P. K. Das, *J. Phys. Chem.*, 1995, **99**, 17891.
23 S. K. Kurtz, *J. Appl. Phys.*, 1968, **39**, 3798.
24 P. Ghosh, S. S. Gupta and P. K. Bharadwaj, *J. Chem. Soc., Dalton Trans.*, 1997, 935.
25 (*a*) P. Ghosh and P. K. Bharadwaj, *J. Chem. Soc., Dalton Trans.*, 1997, 2673; (*b*) D. K. Chand and P. K. Bharadwaj, *Inorg. Chem.*, 1996, **35**, 3380.
26 (*a*) K. Clays and A. Persoons, *Phys. Rev. Lett.*, 1991, **66**, 2980; (*b*) K. Clays and A. Persoons, *Rev. Sci. Instrum.*, 1992, **63**, 3285; (*c*) K. Clays and A. Persoons, *A. Adv. Chem. Phys.*, 1993, **3**, 456.
27 B. J. Orr and J. Ward, *Mol. Phys.*, 1971, **20**, 513.
28 K. Venkatesan and V. Ramamurthy, *Photochemistry in organized and constrained media*, VCH Publishers Inc, New York, 1991, pp. 133–184.